



ISTITUTO NAZIONALE DI RICERCA METROLOGICA
Repository Istituzionale

Heterogeneous nucleation and heat flux avalanches in La(Fe, Si)₁₃ magnetocaloric compounds near the critical point

Original

Heterogeneous nucleation and heat flux avalanches in La(Fe, Si)₁₃ magnetocaloric compounds near the critical point / Bennati, C., Gozzelino, L., Olivetti, E.S., Basso, V.. - In: APPLIED PHYSICS LETTERS. - ISSN 0003-6951. - 109:23(2016), p. 231904. [10.1063/1.4971360]

Availability:

This version is available at: 11696/54603 since: 2021-03-08T15:54:14Z

Publisher:

AIP

Published

DOI:10.1063/1.4971360

Terms of use:

This article is made available under terms and conditions as specified in the corresponding bibliographic description in the repository

Publisher copyright

(Article begins on next page)

Heterogeneous nucleation and heat flux avalanches in $\text{La}(\text{Fe}, \text{Si})_{13}$ magnetocaloric compounds near the critical point

C. Bennati, L. Gozzelino, E. S. Olivetti, and V. Basso

Citation: [Applied Physics Letters](#) **109**, 231904 (2016); doi: 10.1063/1.4971360

View online: <http://dx.doi.org/10.1063/1.4971360>

View Table of Contents: <http://scitation.aip.org/content/aip/journal/apl/109/23?ver=pdfcov>

Published by the [AIP Publishing](#)

Articles you may be interested in

[Relation between paramagnetic entropy and disordered local moment in \$\text{La}\(\text{Fe}_{0.88}\text{Si}_{0.12}\)_{13}\$ magnetocaloric compound](#)

APL Mater. **4**, 064108 (2016); 10.1063/1.4953434

[Shape-anisotropic heterogeneous nucleation and magnetic Gibbs-Thomson effect in itinerant-electron metamagnetic transition of \$\text{La}\(\text{Fe}_{0.88}\text{Si}_{0.12}\)_{13}\$ magnetocaloric compound](#)

Appl. Phys. Lett. **102**, 041913 (2013); 10.1063/1.4789902

[Reversible solid-state hydrogen-pump driven by magnetostructural transformation in the prototype system \$\text{La}\(\text{Fe}, \text{Si}\)_{13}\text{H}_y\$](#)

J. Appl. Phys. **112**, 083918 (2012); 10.1063/1.4759438

[Magnetocaloric materials with first-order phase transition: thermal and magnetic hysteresis in \$\text{LaFe}_{11.8}\text{Si}_{1.2}\$ and \$\text{Ni}_{2.21}\text{Mn}_{0.77}\text{Ga}_{1.02}\$ \(invited\)](#)

J. Appl. Phys. **111**, 07A910 (2012); 10.1063/1.3670987

[Direct measurement of the magnetocaloric effect on \$\text{La}\(\text{Fe}_{13-x-y}\text{Co}_y\)\text{Si}_x\$ compounds near room temperature](#)

J. Appl. Phys. **106**, 023902 (2009); 10.1063/1.3172927



NEW 8600 Series VSM
For fast, highly sensitive
measurement performance

[LEARN MORE](#) 

Heterogeneous nucleation and heat flux avalanches in $\text{La}(\text{Fe}, \text{Si})_{13}$ magnetocaloric compounds near the critical point

C. Bennati,^{1,2} L. Gozzelino,² E. S. Olivetti,¹ and V. Basso¹

¹Istituto Nazionale di Ricerca Metrologica (INRIM), Strada delle Cacce 91, 10135 Turin, Italy

²Department of Applied Science and Technology, Politecnico di Torino, C.so Duca degli Abruzzi 24, 10129 Turin, Italy

(Received 6 September 2016; accepted 21 November 2016; published online 5 December 2016)

The phase transformation kinetics of $\text{LaFe}_{11.41}\text{Mn}_{0.30}\text{Si}_{1.29}\text{H}_{1.65}$ magnetocaloric compound is addressed by low rate calorimetry experiments. Scans at 1 mK/s show that its first order phase transitions are made by multiple heat flux avalanches. Getting very close to the critical point, when the transition becomes of the second order type, the step-like discontinuous behaviour associated with avalanches is smoothed out and the thermal hysteresis disappears. This result is confirmed by magneto-resistivity measurements and allows to obtain accurate values of the temperature hysteresis ($\Delta T_{\text{hyst}} = 0.37$ K) at zero external magnetic field and of the critical field ($H_c = 1.19$ T). The number and magnitude of heat flux avalanches change as the magnetic field strength is increased, showing the interplay between the intrinsic energy barrier between phases and the microstructural disorder of the sample. *Published by AIP Publishing.* [<http://dx.doi.org/10.1063/1.4971360>]

A strong attention is nowadays directed to room temperature refrigeration techniques based on the magnetocaloric effect (MCE) because they allow a reduced energy consumption and a lower environmental impact with respect to gas compression technologies.^{1,2} A class of materials which are promising candidates for magnetic cooling, is the one based on the $\text{La}(\text{Fe}, \text{Si})_{13}$ compound.³ These intermetallics show a large MCE because they exploit a sharp drop in magnetization associated with a ferromagnetic (FM) to paramagnetic (PM) phase transition. Near the transition temperature, T_t , magnetic fields of about 2 T can provide an adiabatic temperature variation up to $\Delta T_{\text{ad}} = 7$ K.³ This giant MCE, observed in magnetic transitions of the first order type, implies thermo-magnetic hysteresis as a drawback for applications. Understanding the mechanism which underlies the thermo-magnetic hysteresis is thus of great importance for the modelling of magnetic refrigeration cycles. It is known that the hysteresis width of $\text{La}(\text{Fe}, \text{Si})_{13}$ is influenced by the strength of the magnetic field,⁴ by hydrostatic pressure⁵ and by substitution element at Fe sites. Moreover, as pointed out on several works,^{6,7} and particularly on those regarding $\text{La}(\text{Fe}, \text{Si})_{13}$ based materials,⁸ the transformation process of first order magnetocaloric materials is due to the motion of phase boundaries between FM and PM phases. This motion takes place on a complex energy landscape influenced by several factors. For example, the strains generated by the lattice shrinking at the PM/FM transitions may influence the free energy profile at local site⁹ as well as the magnetic and structural disorder which can block or favour the transition front advance.^{10–12}

We address this issue by investigating the transformation process as a function of temperature of a $\text{LaFe}_{11.41}\text{Mn}_{0.30}\text{Si}_{1.29}\text{H}_{1.65}$ sample, whose phase transition without external magnetic field is on the border between first and second order types.¹³ The thermo-magnetic hysteresis, on the $H - T$ magnetic phase diagram of the compound, disappears at a critical point, represented by a set of coordinates, the critical field and the critical

temperature (H_c, T_c), which will be investigated in our experiments. By exploiting calorimetry experiments at different temperature scan rates (from 1 mK/s up to 100 mK/s), and by using electrical resistivity measurements, we are able to show that the phase transformation is associated to an heterogeneous nucleation/pinning mechanism characterized by a repeatable sequence of heat flux avalanches.⁸ When a constant external magnetic field is applied and the transition is shifted to higher temperatures, the avalanches change in number and decrease in amplitude until they finally disappear above the critical point.

The starting composition is produced by powder metallurgy by Vacuumschmelze GmbH & Co.¹⁴ powders of the ternary La-Fe-Si alloy are blended with Mn-rich powders. The blends are compacted by cold isostatic pressing and sintered at 1353 K, obtaining fully dense materials with a density of about 7.2 g/cm^3 , characterized by $\text{La}(\text{Fe}, \text{Si})_{13}$ grains of several tens of micrometers and a minor amount of impurity phases (i.e., α -Fe grains, La-rich phases,¹⁵ which are below 2% of the volume¹⁰). The ingot, crushed in fragments with a typical size smaller than 1 mm, is then fully hydrogenated to raise the Curie point (about +150 K) and to ensure the long-term stability of the compound.¹⁶ For the experiments, we selected a single fragment of 5.26 mg with a flat surface. To check the compositional spread of the selected fragment over a mm scale, the elemental composition of the magnetocaloric phase was analysed by the Energy Dispersive X-ray Spectroscopy (EDS) with a ZAF standardless quantification routine. The results of elemental semi-quantitative analysis are reported in Table I. The standard deviation measured for Mn, which is the element present in lower concentration in the sample, and the most influential on the transition temperature, is 5% relative, which is compatible with the repeatability limit obtained on standard specimens of metallic alloys of known and uniform composition.¹⁷ This suggests that the actual compositional spread of the analysed sample (instrumental and counting statistics factors excluded) is negligible and the magnetocaloric phase of the studied fragment is expected to have a single transition temperature.

TABLE I. Atomic % composition of the main MCE phase of the investigated samples: nominal values are compared to the microanalysis values obtained on the selected fragment. Hydrogen atoms cannot be detected by the EDS technique.

| LaFe _{11.41} Mn _{0.30} Si _{1.29} H _{1.65} | | | | |
|---|------|------|------|------|
| at. % | La | Fe | Mn | Si |
| Nominal values | 7.14 | 81.5 | 2.14 | 9.21 |
| Measured values | 7.4 | 79.6 | 2.1 | 10.9 |
| St.dev. | 0.2 | 0.5 | 0.1 | 0.5 |

The experiments as a function of temperature were performed employing a differential scanning calorimeter based on two Peltier cells, a reference one and the sample holder, on which the specimen has been attached with a silver paint.¹⁸ The two cells are connected differentially in order to subtract the common heat flux background, thus the heat flux exchanged with the sample is computed from the voltage difference measured at the end of the two cells. The important quantities returned from the calorimeter are the heat flux, q_s , and the temperature of the sample holder, T_p .¹⁹ Electrical measurements were performed, on the same sample, in a two stage cryogen-free cryocooler, using a standard four point technique and monitoring the temperature of the cryostat by a CernoxTM thermometer.

Zero magnetic field transitions obtained by calorimetric measurements while controlling and varying the thermal bath temperature, T , at different heating rates ($dT/dt = 100$ mK/s, 50 mK/s, 20 mK/s, and 1 mK/s) are presented in Fig. 1(a). In this plot, the transition width ($\Delta T = T_{start} - T_{end}$) tends to reduce at lower scan rates, for which different peaks become observable during the transition process. By using time on the horizontal-axis, this feature becomes more clear. Fig. 1(b) shows how, slowing down dT/dt , the heat flux signal becomes structured into a succession of individual transformation events. These isolated events are not visible in the faster (>50 mK/s) scans, suggesting that they are related to sudden transformations of volume occurring at temperatures very close together. Fig. 1(c) shows the plots of T and of the sample holder temperature, T_p , as a function of time for the same heating sequence of Figs. 1(a) and 1(b). Away from the transition region, the lag between the two temperatures is constant depending only on the scanning rate and it becomes very small for the 1 mK/s measurements. The equation governing these differences is given by

$$T - T_p = \tau_p \frac{dT}{dt}, \quad (1)$$

where $\tau_p = 2.6$ s is a time constant introduced by the measuring Peltier cells, determined by proper calibration experiments.¹⁹ Only the lower rate permits to observe that, in the transition region, T_p has sudden drops, similarly to overheating processes, which are likely associated to switches between metastable states inside the volume of the sample. When an avalanche starts and the sample begins to transform, T_p rapidly decreases of several mK, imaging a fast absorption of heat from the sample. After that the whole system tends to restore an equilibrium with the thermal bath

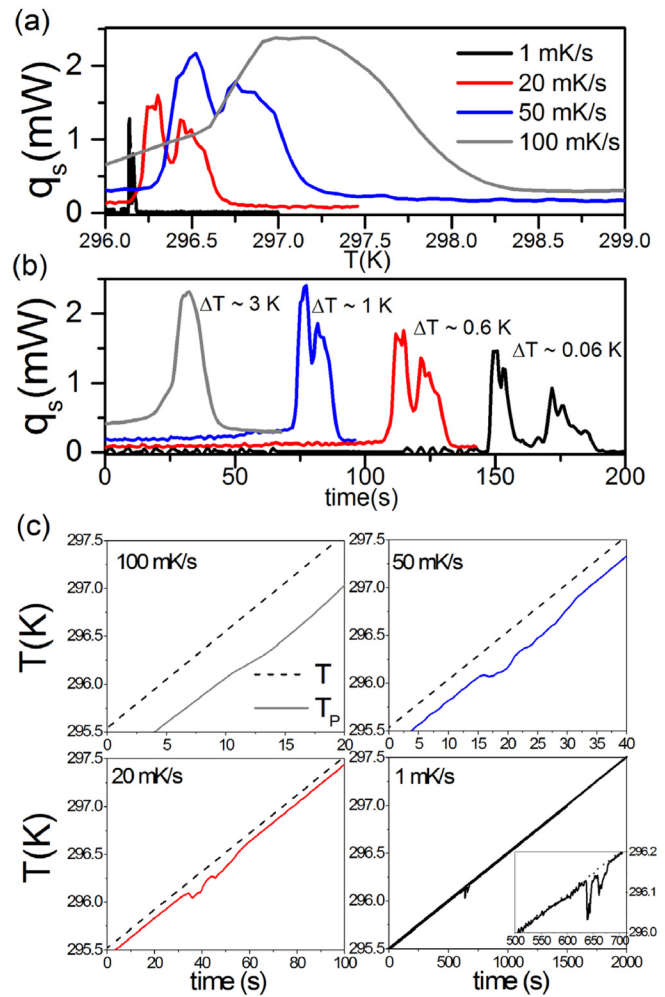


FIG. 1. (a) Temperature induced phase transitions at different scanning rates as a function of the thermal bath temperature (a). The magnetic field is fixed at $H = 0$. (b) The same measurements are plotted as a function of time. ΔT values represent temperature widths of each transition as obtained from (a). Time values are translated to permit the complete visualization of all the transitions. (c) Temperature as a function of time for different scanning rates (100, 50, 20, and 1 mK/s) on heating: T is the temperature of the thermal bath—monitored by a Pt100 thermometer, whereas T_p is the temperature of the sample holder.

temperature. The multiple peaks signal may be due to different factors, for example, slight differences in the composition across the volume giving rise to a distribution of transition temperatures²⁰ (i.e., each piece behaves independently⁶). Furthermore, the microstructural disorder (grain boundaries, magnetic and non magnetic precipitated phases) may locally modify the energy landscape facing the phase front, representing nucleation and/or pinning sites^{8,21} (i.e., the transition is affected by the microstructure rather than by compositional spread¹²). The effective entropy changes, computed for the four scan rates, are compared in Fig. 2. The relative thermal hysteresis were calculated from the temperature of onset and at the end of each transition in the case of low scanning rate, and by the inflection point method for the faster rate cases.¹³

A linear fit of thermal hysteresis versus the scanning rate (inset graph at Fig. 2) yields a ‘zero rate’ hysteresis of the compound of 0.37 K. This value is smaller but close to 0.4 K obtained for agglomerated fragments (total mass = 50 mg) of

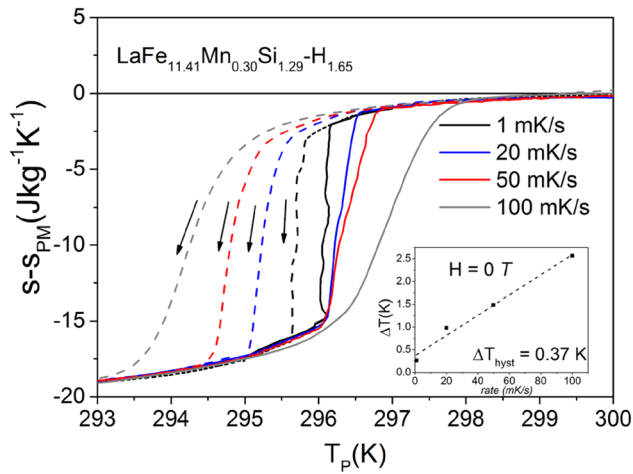


FIG. 2. Total entropy change of the transition at different applied scanning rates (100, 50, 20, and 1 mK/s), down arrows indicate the cooling curves. Inset: thermal hysteresis in OH as a function of the temperature scanning rate. S_{PM} is the entropy of the paramagnetic state (obtained by fixing the specific heat of the paramagnetic phase at $465 \text{ J kg}^{-1} \text{ K}^{-1}$).¹³

the same material closed in an aluminium pan.¹³ Moreover, the ΔS value stays nearly unchanged independent of the rate of scan, but at 1 mK/s, the entropy follows a re-entrant hysteresis loop as a function of T_p . This effect reflects either the multi-avalanche heat flux signal of Figs. 1(a) and 1(b) and the plot of temperature vs time of Fig. 1(c), allowing to conclude that the low rate technique can be used either to quantify the important MCE quantities of the material and, in addition, to observe the microscopic details of the phase transition.^{22,23}

In order to deepen the latter point, the evolution of the avalanches as a function of temperature was studied by applying different magnetic fields, being able to cross the critical point for which the transition becomes of the second order.¹³ The top graph on Fig. 3(a) displays the transitions as a function of T on heating (FM to PM, endothermic) and on cooling (PM to FM, exothermic) obtained in magnetic fields of 0, 0.4, 1.0, and 1.4 T. Two main features appear with the field: (i) the avalanches change in number and in magnitude, (ii) a continuous background gradually substitutes the heat flux content of the peaks masking the starting and ending point of each avalanche event and also widening the transition. The heating sequence plotted as a function of time in Fig. 3(b) shows how the heat flux avalanches are gradually suppressed by the magnetic field. The cooling sequence of Fig. 3(c) is analogous to the heating one and, correspondingly, it shows a redistribution and a gradual reduction of the heat flux avalanches with increasing field. The falling magnitude of the peaks reflects both the lowering of the latent heat content of the transition²⁰ and, consequently, the gradual reduction of the overall free energy barrier between the FM and the PM phase⁴ with field. Beside their magnitude values, we observe that the avalanches corresponding to the measurements performed under higher values of the applied magnetic field, do not appear as just shifted in temperature with respect to zero-field avalanches. According to the EDS results, we can thus exclude a significant graded distribution of the transition temperature due to non uniform chemical compositions. Instead, we suppose a nucleation mechanism which changes relevantly near the critical point (H_c, T_c).

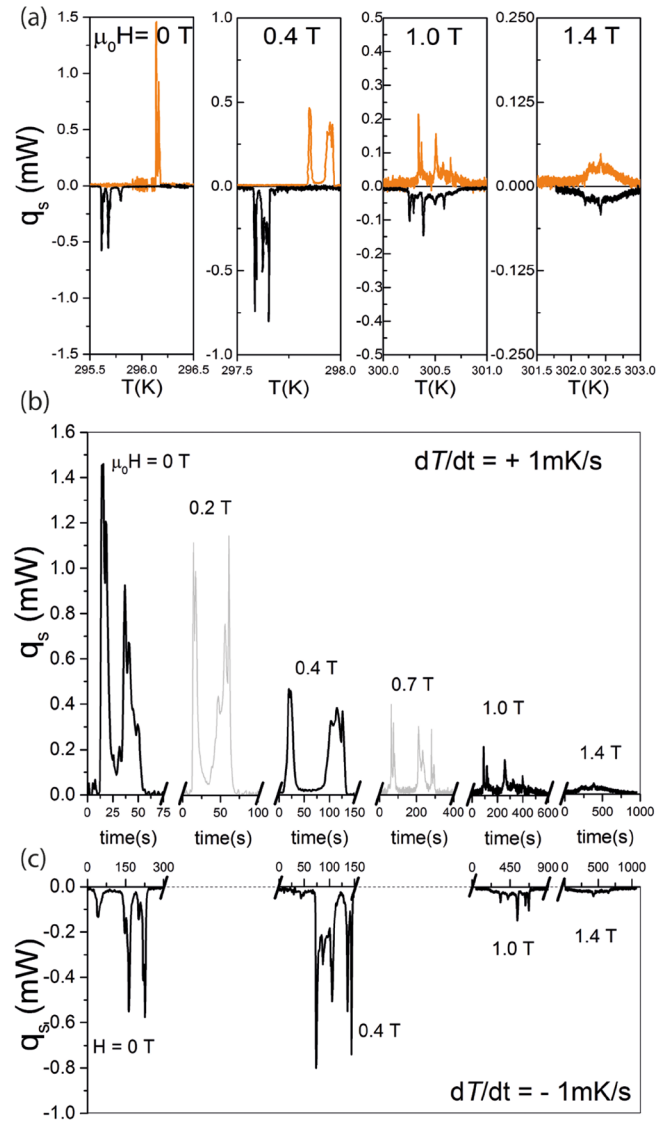


FIG. 3. (a) Temperature induced phase transitions at different applied magnetic fields as a function of the temperature of thermal bath, T ; Heating curves are depicted in orange, cooling curves in black. The scanning rate is 1 mK/s. (b) and (c) heating and cooling, respectively, temperature-induced phase transitions at different applied magnetic fields as a function of time. Time has been translated to permit the complete visualization of the transitions.

We interpret the varying number of avalanches as follows: grain boundaries, precipitated phase or other sources of disorder are preferential nucleation sites and are randomly distributed into the sample; if the energy of the system, driven by temperature, overwhelms the local energy barrier between phases at these sites, an avalanche can be set off. By reducing the overall intrinsic energy barrier with field, a new modulation of the local energies values is expected, and the avalanches in our experiments change: they increase in number and decrease in amplitude. The local energy barrier to overcome indeed depends on both the intrinsic PM/FM energy barrier (characteristic of the compound) and on the local disorder (characteristic of the sample). In such a picture, approaching the critical point, the decreased FM/PM (PM/FM) free-energy barrier takes advantage of local fluctuations.²¹ As a consequence of the overall decrease of the intrinsic energy barrier, the thermal hysteresis of the compound, computed from the entropy change as a function of

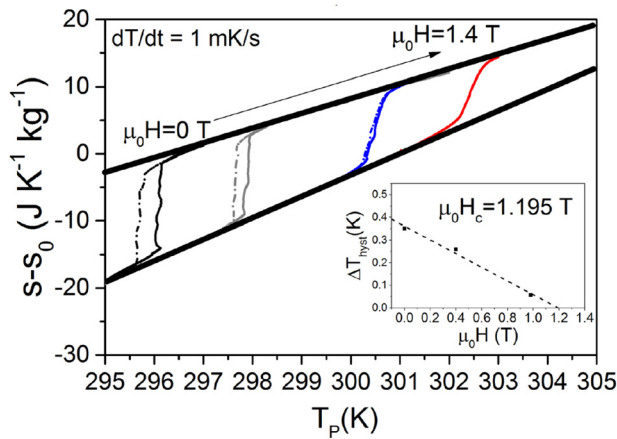


FIG. 4. Entropy changes at the temperature induced phase transitions in different applied magnetic fields as a function of temperature; scanning rates is 1 mK/s. The entropy change was calculated as $s - s_0$, where s_0 is the reference entropy given by the entropy without magnetic field at the reference temperature $T_m = 296.5$ K, above the transition temperature. Inset: the relative thermal hysteresis as a function of the magnetic field calculated from the onset temperature of first avalanches.

the magnetic field, reduces (Fig. 4). The absence of hysteresis at 1.4 T (red curve) can be compared to the last graph of Fig. 3(a) where a small avalanche peak is still detectable with the calorimetry scan. This fact highlights the tiny balance existing among the energy scales involved at the transition: the one regarding local perturbation and the one due to the intrinsic energy barrier between phases. When the last one is almost null (i.e., in the proximity of the critical point), we suggest that the local disorder appears irrelevant for the transformation dynamics. The reproducibility of these results is reported from measurements performed on another fragment of mass 4.53 mg of the same composition. Repeated low rate scans are reported in Fig. 5. The left and right couples of scans, taken at

zero and at 0.87 T, respectively, show small differences from measurement to measurement, demonstrating that the avalanches are not random, probably depending only on the unique local energy landscape of each sample. The slight changes in the peak temperatures are mainly ascribable to the experimental uncertainty of T and H and to the sampling time (0.75 s).¹⁹

For completeness, the temperature dependence of the electrical resistivity, ρ , at different applied magnetic fields was also measured, and the results are plotted in Fig. 6. The FM and PM phases have different values of ρ , mainly ascribable to the larger cubic cell of the low temperature phase,^{24,25} thus that any transformed fraction of the volume can be thought as a new resistive element in the measurements. It is worth to observe that transitions below 1 T (a value which is below the critical magnetic field of 1.29 ± 0.17 T) show detectable jumps in ρ , which are again a sign of the heterogeneous transformation of volumes inside the sample. The temperature hysteresis computed from entropy changes at $\mu_0 H \neq 0$ (Fig. 4) provides a critical field value of about $\mu_0 H_c = 1.195$ T (inset graph). This value and the one obtained from faster rates measurements ($H_c = 1.3$ T¹³) agree within the experimental errors with that obtained from electrical resistivity (the critical magnetic field is about 1.29 ± 0.17 T). The lowest $\mu_0 H_c$ has been obtained by low calorimetric experiments as well as the most precise value of the $\Delta T_{hyst} = 0.37$ K at zero external applied magnetic field.

We have thus shown, that the thermodynamic quantities of interest for magneto cooling cycles can be obtained with confidence by using different experimental detection techniques also when transitions are of the first order type. Going into the details of the transitions, we have shown that the evolution of the first order transitions in our $\text{La}(\text{Fe}, \text{Si})_{13}$ based material is characterized by an avalanches-like behaviour. These bursty events show up in different samples and can be isolated by using sufficiently low temperature scan

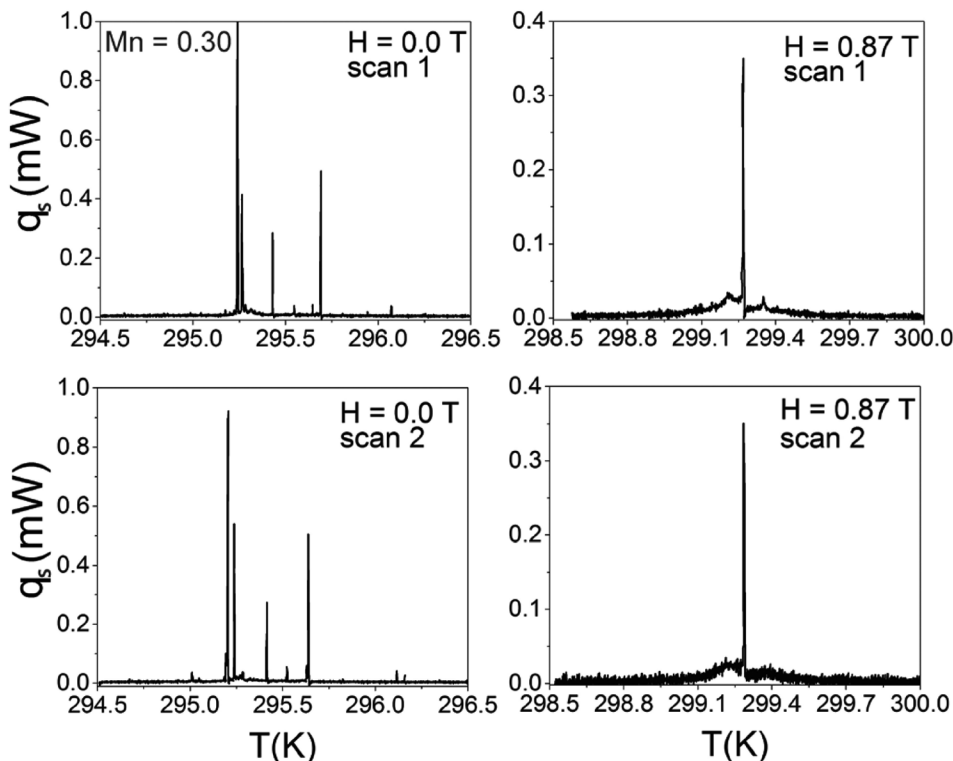


FIG. 5. Repeated temperature scans performed at two magnetic fields (left graphs $H = 0.0$ T and right graphs $H = 0.87$ T) in different moments of the acquisition procedure. These measurements belong to a second fragment (mass 4.53 mg) of the $\text{LaFe}_{11.41}\text{Mn}_{0.30}\text{Si}_{1.29}\text{H}_{1.65}$ composition, taken from the large scale production of Vacuumschmelze GmbH.

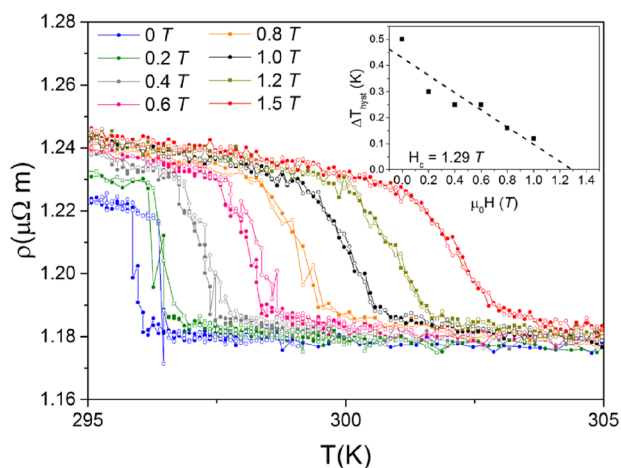


FIG. 6. Electrical resistivity behaviour at temperature induced phase transitions in different applied magnetic fields as a function of temperature; scanning rate is ~ 3.5 mK/s. Inset: the relative thermal hysteresis as a function of the magnetic field.

rate. We showed how avalanches change depending on whether the temperature and magnetic field of transition are close to or far from the critical point. The 1 mK/s rate used in our experiments also highlighted a strong interplay between the intrinsic energy barrier between phases, responsible for the first order character of the transition, and the structural disorder, characterizing each sample. This finding opens up further questions on the kinetics of the phase transition, disclosing the existence of a rough and complex energy landscape which is critical in determining the onset of transitions and the hysteresis width in $\text{La}(\text{Fe}, \text{Si})_{13}$ based compounds. We suggest that, below the critical point, it might be possible to study in detail the typical avalanche sizes, their number, and their relation with the latent heat content of first order phase transitions. For this purpose, a theoretical modeling aimed to describe the avalanches, and their relevance to the dynamic behaviour of the magnetocaloric effect is underway. The model should take into account the fact that the free energy of each system depends on both the intrinsic barrier separating the magneto-structural phases, which decrease toward the critical point, as well as on its local perturbations induced by quenched disorder.

The authors thank M. Katter and A. Barzca from Vacuumschmelze GmbH, Germany, for providing the $\text{La}(\text{Fe}-\text{Mn}-\text{Si})-\text{H}$ samples.

- ¹J. Liu, T. Gottschall, K. P. Skokov, J. D. Moore, and O. Gutfleisch, *Nat. Mater.* **11**, 620 (2012).
- ²O. Tegus, E. Brück, K. Buschow, and F. De Boer, *Nature* **415**, 150 (2002).
- ³S. Fujieda, A. Fujita, and K. Fukamichi, *Appl. Phys. Lett.* **81**, 1276 (2002).
- ⁴A. Fujita, S. Fujieda, K. Fukamichi, H. Mitamura, and T. Goto, *Phys. Rev. B* **65**, 014410 (2001).
- ⁵A. Fujita and H. Yako, *Scr. Mater.* **67**, 578 (2012).
- ⁶K. Morrison, J. Moore, K. Sandeman, A. Caplin, and L. Cohen, *Phys. Rev. B* **79**, 134408 (2009).
- ⁷R. Niemann, S. Hahn, A. Diestel, A. Backen, L. Schultz, K. Nielsch, M.-X. Wagner, and S. Fähler, *APL Mater.* **4**, 064101 (2016).
- ⁸M. Kuepferling, C. Bennati, F. Laviano, G. Ghigo, and V. Basso, *J. Appl. Phys.* **115**, 17A925 (2014).
- ⁹A. Waske, L. Giebeler, B. Weise, A. Funk, M. Hinterstein, M. Herklotz, K. Skokov, S. Fähler, O. Gutfleisch, and J. Eckert, *Phys. Status Solidi RRL* **9**, 136 (2015).
- ¹⁰C. Bennati, F. Laviano, G. Durin, E. Olivetti, V. Basso, G. Ghigo, and M. Kuepferling, *J. Magn. Magn. Mater.* **400**, 339 (2015).
- ¹¹S. J. Kim, K. J. Lee, M. H. Jung, H. J. Oh, and Y. S. Kwon, *J. Magn. Magn. Mater.* **323**, 1094 (2011).
- ¹²A. Waske, E. Lovell, A. Funk, K. Sellschopp, A. Rack, L. Giebeler, P. Gostin, S. Fähler, and L. Cohen, *APL Mater.* **4**, 106101 (2016).
- ¹³V. Basso, M. Kuepferling, C. Curcio, C. Bennati, A. Barzca, M. Katter, M. Bratko, E. Lovell, J. Turcaud, and L. F. Cohen, *J. Appl. Phys.* **118**, 053907 (2015).
- ¹⁴A. Barzca, M. Katter, V. Zellmann, S. Russek, S. Jacobs, and C. Zimm, *IEEE Trans. Magn.* **47**, 3391 (2011).
- ¹⁵M. Katter, V. Zellmann, G. W. Reppel, and K. Uestuener, *IEEE Trans. Magn.* **44**, 3044 (2008).
- ¹⁶M. Krautz, K. Skokov, T. Gottschall, C. S. Teixeira, A. Waske, J. Liu, L. Schultz, and O. Gutfleisch, *J. Alloys Compd.* **598**, 27 (2014).
- ¹⁷ASTM E1508-12, *Standard Guide for Quantitative Analysis by Energy-Dispersive Spectroscopy* (ASTM International, 1998).
- ¹⁸M. Kuepferling, C. Sasso, and V. Basso, in *EPJ Web of Conferences* (EDP Sciences, 2013), Vol. 40, p. 06010.
- ¹⁹V. Basso, C. P. Sasso, and M. Kuepferling, *Rev. Sci. Instrum.* **81**, 113904 (2010).
- ²⁰K. Morrison, J. Lyubina, J. Moore, A. Caplin, K. Sandeman, O. Gutfleisch, and L. Cohen, *J. Phys. D: Appl. Phys.* **43**, 132001 (2010).
- ²¹Y. Imry and M. Wortis, *Phys. Rev. B* **19**, 3580 (1979).
- ²²J. Moore, K. Morrison, K. Sandeman, M. Katter, and L. Cohen, *Appl. Phys. Lett.* **95**, 252504 (2009).
- ²³E. Lovell, A. M. Pereira, A. D. Caplin, J. Lyubina, and L. F. Cohen, *Adv. Energy Mater.* **5**(6), 5 (2015).
- ²⁴T. Palstra, J. Mydosh, G. Nieuwenhuys, A. Van der Kraan, and K. Buschow, *J. Magn. Magn. Mater.* **36**, 290 (1983).
- ²⁵F. Hu, J. Gao, X. Qian, Y. Li, J. Du, J. Sun, and B. Shen, *IEEE Trans. Magn.* **40**, 2754 (2004).